



Bioremediation in marine ecosystems: a computational study combining ecological modelling and flux balance analysis

Marianna Taffi, Nicola Paoletti, Claudio Angione, Sandra Pucciarelli, Mauro Marini and Pietro Lio

Journal Name:	Frontiers in Genetics
ISSN:	1664-8021
Article type:	Original Research Article
First received on:	04 Jun 2014
Revised on:	09 Aug 2014
Frontiers website link:	www.frontiersin.org



1

Bioremediation in marine ecosystems: a computational study combining ecological modelling and flux balance analysis

Marianna Taffi^{1,*}, Nicola Paoletti², Claudio Angione³, Sandra Pucciarelli¹, Mauro Marini⁴, and Pietro Liò³

¹*School of Biosciences and Veterinary Medicine, University of Camerino, Camerino, Italy*

²*Department of Computer Science, University of Oxford, Oxford, United Kingdom*

³*Computer Laboratory, University of Cambridge, Cambridge, United Kingdom*

⁴*National Research Council, Institute of Marine Science, Ancona, Italy*

Correspondence*:

Marianna Taffi

School of Biosciences and Veterinary Medicine, University of Camerino, Via Gentile III Da Varano, 62032 Camerino, Italy, marianna.taffi@unicam.it

2 ABSTRACT

3 The pressure to search effective bioremediation methodologies for contaminated ecosystems has led
4 to the large-scale identification of microbial species and metabolic degradation pathways. However,
5 minor attention has been paid to the study of bioremediation in marine food webs and to the definition
6 of integrated strategies for reducing bioaccumulation in species. We propose a novel computational
7 framework for analysing the multiscale effects of bioremediation at the ecosystem level, based
8 on coupling food web bioaccumulation models and metabolic models of degrading bacteria. The
9 combination of techniques from synthetic biology and ecological network analysis allows the specification
10 of arbitrary scenarios of contaminant removal and the evaluation of strategies based on natural or
11 synthetic microbial strains. In this study, we derive a bioaccumulation model of Polychlorinated biphenyls
12 (PCBs) in the Adriatic food web, and we extend a metabolic reconstruction of *Pseudomonas putida*
13 KT2440 (iJN746) with the aerobic pathway of PCBs degradation. We assess the effectiveness of different
14 bioremediation scenarios in reducing PCBs concentration in species and we study indices of species
15 centrality to measure their importance in the contaminant diffusion via feeding links. The analysis of the
16 Adriatic sea case study suggests that our framework could represent a practical tool in the design of
17 effective remediation strategies, providing at the same time insights into the ecological role of microbial
18 communities within food webs.

19 **Keywords:** PCBs; Bioremediation; Adriatic Sea; *Pseudomonas Putida*; Flux Balance Analysis; Ecological Network Analysis

1 INTRODUCTION

20 Aquatic ecosystems are subject to a mixture of synthetic organic chemicals, leading to adverse effects
21 on organisms at different levels of biological organization and at all trophic levels of the food web. Over
22 the last decades, many removal strategies have been proposed in order to reduce the bioavailability of
23 *Persistent Organic Pollutants* (POPs) and to limit the consequent bioaccumulation phenomena on species.
24 *Polychlorinated biphenyls* (PCBs) are a class of POPs consisting of 209 different congeners, obtained from

25 the catalytic chlorination process of biphenyl, and characterized by high environmental persistence and
26 resistance to natural ways of breakdown. PCBs are practically insoluble in water and due to their lipophilic
27 nature, they easily dissolve in fats and lipids causing bioaccumulation, i.e. the phenomenon by which the
28 internal contaminant concentration of an organism is higher than in the external medium. Indeed, PCBs
29 have been detected both in aquatic biota and in all the abiotic phases of marine environments (sediments,
30 water and dissolved organic carbon). Generally, heavier chlorinated PCBs congeners tend to accumulate
31 in oxygen-depleted zones of sediments. Moreover, they bioconcentrate in species by following biomass
32 flows in predator-prey relationships. PCBs bioaccumulation phenomena in aquatic organisms occur over
33 time as the result of multiple contamination pathways, including processes of uptake (e.g. dietary and
34 dermal absorption) and elimination (e.g. egestion and respiration).

35 However, not all the living organisms in a polluted environment are prone to bioaccumulation. The
36 sizeable variety of marine microbial life is metabolically involved in many transformation processes
37 like biogeochemical cycles of elements, water quality conservation and biodegradation of many organic
38 pollutants. Microbial communities are also an active compartment at the lower trophic levels of marine
39 food webs. They interact with the grazing activities of planktonic groups and play a crucial role in the
40 mineralization of organic matter through the complex trophic pathway known as the *microbial loop*
41 (Fenchel, 2008). The bioremediation of PCBs is biologically incomplete, since it takes place via two
42 distinct microbially mediated processes: anaerobic bacteria by reductive dechlorination remove chlorine
43 atoms in higher chlorinated congeners, which are then oxidatively reduced by aerobic bacteria via
44 cometabolic reactions (Brown Jr et al., 1987; Bedard and Quensen III, 1995). Even if PCBs are difficult
45 to fully degrade, the patterns of PCBs mixtures can potentially lead to the development of novel catabolic
46 pathways, thus increasing the genetic microbial variability in the aquatic ecosystem (Pieper and Reineke,
47 2000; Lovley, 2003).

48 Computational models and predictive tools have found wide applicability and usefulness both in
49 ecotoxicological studies and in the genome-scale reconstruction of pollutant degrading bacteria. However,
50 to the best of our knowledge, these techniques have never been considered for investigating, in a combined
51 way, the multiscale effects of microbial bioremediation at the ecological level. In this work, we develop
52 a computational framework that integrates bioaccumulation information at ecosystem level with genome-
53 scale metabolic models of degrading bacteria. We apply it to the case study of the PCBs bioremediation
54 in the Adriatic food web.

55 Specifically, we estimate the PCBs bioaccumulation model by using Linear Inverse Modelling, and we
56 employ Flux Balance Analysis to extend the metabolic reconstruction of the toluene degrading bacteria
57 *Pseudomonas putida* KT2440 (iJN746) presented in Nogales et al. (2008) with the aerobic pathway of
58 PCBs degradation. We also provide a general method to obtaining integrated ecological-metabolic models,
59 relying on a reaction-based encoding of the food web and on the definition of different bioremediation
60 scenarios. We analyse the effects of varying oxygen levels on the microbial growth and on the PCBs
61 uptake of the extended *P. putida* by means of bilevel optimization to evaluate the efficiency of biomass
62 production when PCBs uptake is favoured and when interactions with the toluene degradation pathway
63 are considered. Finally, we apply ecological network analysis tools to study structural properties of the
64 bioaccumulation networks obtained at increasing degrees of bioremediation efficiency. By testing different
65 bioremediation interventions, our computational experiments provide insights into the potential reduction
66 of bioconcentration in the food web, into the role of species in the diffusion of PCBs, and ultimately, into
67 the overall status of ecosystem sustainability.

2 METHODS

2.1 ESTIMATION OF PCBS BIOACCUMULATION IN THE ADRIATIC SEA

68 In our framework we focus on the case of PCBs bioaccumulation in the Adriatic sea, a semi-enclosed
69 basin characterized by high biodiversity (Coll et al., 2010; Danovaro et al., 2010) and by the presence

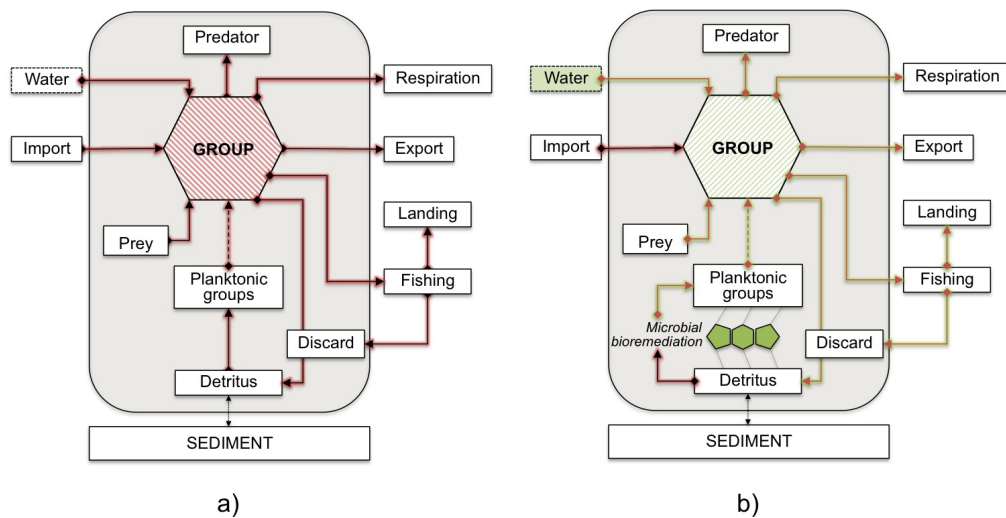


Figure 1. Conceptual model of the Adriatic PCBs bioaccumulation network. Flows are shown with respect to a generic functional group. Mass-balanced groups are enclosed in the gray boxes, externals are shown outside. The dashed arrow from planktonic groups indicate possible indirect connections. Feeding links from discard and detritus are omitted. a) red arrows indicate contaminant flows mediated by feeding connections. b) green arrows highlight the potential propagation of bioremediation effects. Possible bioremediation scenarios are assumed at the interface between detritus and planktonic groups (microbial loop), or in the water compartment.

70 of multiple contamination sources and anthropogenic perturbations. In the last decades different species
 71 of ecological and commercial interest have been surveyed in this region and several toxicological studies
 72 report the occurrence of PCBs bioaccumulation in Adriatic sea (Storelli et al., 2007; Perugini et al.,
 73 2004; Marcotrigiano and Storelli, 2003; Bayarri et al., 2001; Corsolini et al., 2000; Sagratini et al.,
 74 2008). We consider the PCBs bioaccumulation model presented in (Taffi et al., under revision¹) where
 75 a review of bioaccumulation studies in the North, Central and South Adriatic sea (period 1994-2002) is
 76 conducted in order to estimate bioconcentrations and PCBs flows among species. The model consists of
 77 39 functional groups and is defined on top of a trophic reconstruction obtained from data collected in Coll
 78 et al. (2007), one of the most complete quantitative studies of the Northern and Central Adriatic food web.

79 We assume that organic chemicals follow the same paths as biomasses, moving via feeding link through
 80 the trophic structure of the food web, which is a common approach in the field of ecotoxicological
 81 modelling (Christensen and Walters, 2004; Hendriks et al., 2001; Laender et al., 2009). Flow rates
 82 quantify the intensity at which the contaminant is transferred from the source to the target (i.e. from prey to
 83 predator), and are estimated at mass-balance conditions from bioconcentration and biomass values of the
 84 involved groups. We also include external unbalanced compartments, implementing potentially unlimited
 85 exogenous imports and exports. Network estimation is achieved through *Linear Inverse Modelling (LIM)*
 86 (van Oevelen et al., 2010), used to compute flow rates and bioconcentrations (the unknowns) by solving
 87 a system of linear constraints that incorporate empirical bioaccumulation data. If constraints are not
 88 contradictory, there are generally multiple admissible values that can be chosen. In our case, we derive
 89 a statistically well-founded solution by taking the mean² of a set of random solutions obtained with
 90 Monte-Carlo sampling.

91 Figure 1 illustrates the conceptual model and the topology of our PCBs bioaccumulation network; in
 92 Table 1, we provide a description of the contaminant flows and of the constrains used for their estimation.
 93 We consider the sum of PCBs congeners, expressed in ng g^{-1} wet weight-based. Biomasses are measured

¹ A recent version is available at <http://arxiv.org/abs/1405.6384>

² Being a linear operation, the mean of valid solutions to a system of linear constraints is in turn a valid solution to the system (see also van Oevelen et al. (2010)).

Table 1. Main flows in the PCBs bioaccumulation network and linear constraints for their estimation from data.

<p>Mass balances: $\sum_j c_{j \rightarrow i} - \sum_j c_{i \rightarrow j} = 0$ The bioconcentration of a generic group i is estimated under the mass-balance assumption; j ranges among groups and external compartments¹.</p>
<p>Concentration data: $C_i \propto k$ where k is an input PCBs value used to constrain concentration C_i and $\propto \in \{=, \leq, \geq\}$. Note that an arbitrary number of data constraints can be included for the same group.</p>
<p>Uptake from food/losses: $c_{j \rightarrow i} = b_{j \rightarrow i} \cdot C_j$ The contaminant flow from group j to i is the product of the corresponding biomass flow $b_{j \rightarrow i}$ and the PCBs concentration in the source j. This equation characterizes both the contaminant uptake of predator i by consumption of prey j and the contaminant removal from j due to predation by i. If instead i is an external, the equation can express generic outflows to the export compartment ($c_{j \rightarrow \text{Export}}$); respiration flows ($c_{j \rightarrow \text{Respiration}}$), which account for part of the unassimilated fraction of ingested biomass; or removal due to fishing activity, which can be directed to the landings ($c_{j \rightarrow \text{Landing}}$) or to the discards ($c_{j \rightarrow \text{Discard}}$). The latter enters back the biomass cycle and is modelled as a mass-balanced group, with its own bioconcentration value.</p>
<p>Uptake from generic imports: $c_{\text{Import} \rightarrow i} = b_{\text{Import} \rightarrow i} \cdot C_i$ This class of constraints describes generic imports of PCBs coming from external contaminant inflows (e.g. immigration), which we group in the Import compartment. In this case, the PCBs concentration in the biomass imported into group i is assumed to be the same as in i.</p>
<p>Uptake from environment: $c_{\text{Water} \rightarrow i} = w_i \cdot C_{\text{Water}}$ where w_i is the rate of contaminant uptake from water by group i and C_{Water} is the concentration in water². Contaminant uptakes from water are not mediated by a biomass transfer and are estimated according to mass-balance constraints.</p>
<p>Non-negativity of concentrations: $C_i \geq 0$</p>

¹ Natural detritus and planktonic groups are assumed to be in instant equilibrium with the water phase, and their concentration only depends on the concentration in water.

² When also C_{Water} is unknown, the constraint becomes non-linear and w_i cannot be directly estimated. In this case, $c_{\text{Water} \rightarrow i}$ is treated as a single unknown. We assume null w_i for compartments in rapid equilibrium with the water phase.

94 in t km^{-2} wet weight organic matter, and biomass flows in $\text{t km}^{-2} \text{ yr}^{-1}$. PCBs flow rates are thus expressed
95 in $\text{mg km}^{-2} \text{ yr}^{-1}$. We denote the contaminant flow from prey i to predator j with $c_{i \rightarrow j}$, and the PCBs
96 concentration in i with C_i . We assume that biomass flows ($b_{i \rightarrow j}$) are known quantities and are estimated
97 as reported in (Taffi et al., under revision).

2.2 INTEGRATION OF PCBs DEGRADATION PATHWAYS INTO *P. PUTIDA* KT2440

98 Various environmental and biological factors limit the natural PCBs degradation process, among which
99 the high selectivity of bacteria for specific PCBs congeners. Higher chlorinated congeners typically
100 tend to accumulate in marine sediments, where anaerobic bacteria by reductive dechlorination use
101 these compounds as alternative electron acceptors in their respiration processes, thus making PCBs
102 less chlorinated and more aerobically degradable. This step is generally slow but crucial in the whole
103 detoxification process, and various PCBs-dechlorinating bacteria, mainly belonging to the phylum
104 *Chloroflexi*, have been isolated and characterized in different contaminated sites (Fava et al., 2003).
105 The bioconversion process of less chlorinated PCBs congeners is performed by aerobic bacteria able
106 to oxidatively cometabolize PCBs as the unique carbon source, since they encode biphenyl-metabolic
107 enzymes (*bph*). In order to have an effective degradation process, this aerobic step should ideally take
108 place sequentially to the anaerobic step in the full microbial degradation pathway. As illustrated in Figure

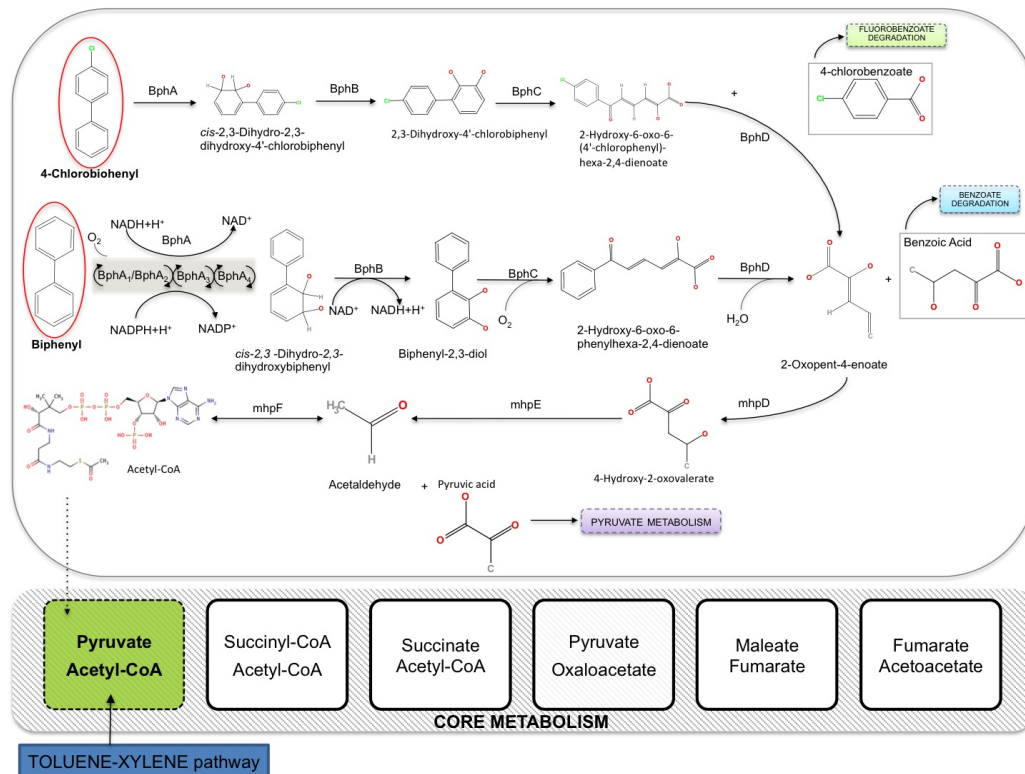


Figure 2. Integration of the aerobic pathway of PCBs degradation in the core metabolism of *P. putida* KT2440 (iJN746). BphA=biphenyl 2,3-dioxygenase (multicomponent Rieske non-heme iron oxygenases); BphB=cis-2,3-dihydrobiphenyl-2,3-diol dehydrogenase; BphC=biphenyl-2,3-diol 1,2-dioxygenase; BphD=2,6-dioxo-6-phenylhexa-3-enoate hydrolase; mhpD=2-keto-4-pentenolate hydratase; mhpE=4-hydroxy 2-oxovalerate aldolase; mhpF=acetaldehyde dehydrogenase.

109 2, the established aerobic route of PCBs elimination involves a set of enzymatic reactions acting on
 110 (chloro)biphenyl congeners to yield first, benzoic acid; and then, pyruvate and acetyl-CoA, molecules
 111 that directly enter the Krebs cycle and allow the microbial biomass growth. Several aerobic bacteria
 112 are environmentally widely present and characterized as belonging to a variety of genera, including
 113 *Pseudomonas putida* (Furukawa, 2000). In particular, strains of *P. putida* have been isolated in water
 114 habitats and marine sediments (Garcia-Valdes et al., 1988).

115 In this work, we construct a synthetic model of PCBs degrading bacteria using the FBA approach
 116 (see Sect. 2.3), by extending the metabolic reconstruction of *P. putida* KT2440 (iJN746) in Nogales
 117 et al. (2008) with the aerobic degradation pathway of PCBs (KEGG pathway: map00621). As explained
 118 above, the pathway connects to the core metabolism of *P. putida* at the starting point of the citrate
 119 cycle (see Fig. 2). The *P. putida* TOL-plasmid has been extensively used as a discovery platform for
 120 bioremediation purposes, since it encodes enzymes required for aromatic hydrocarbons degradation (e.g.,
 121 toluene, benzoate, phenylacetate, nicotinate). Several studies report the genetic plasticity of different
 122 strains of *Pseudomonas spp.*, showing the correspondence between gene clusters involved in biphenyl
 123 degradation pathways (Furukawa and Miyazaki, 1986) and genes for toluene degradation (Furukawa
 124 et al., 1993).

2.3 BILEVEL FLUX BALANCE ANALYSIS

125 Starting from biochemical reactions and stoichiometric coefficients, the Flux Balance Analysis (FBA)
 126 framework is based on the assumption of a metabolic steady state (Orth et al. (2010)). That is, for
 127 each metabolite in the network, a balance is kept between the fluxes of those reaction in which the
 128 metabolite is a reactant, and those in which it is a product. Due to its ability to handle large biochemical
 129 networks without requiring kinetic parameters, FBA allows an effective in silico analysis of the invariant
 130 characteristics of the metabolic network at a low computational cost.

131 Formally, let X_h , $h = 1, \dots, m$ be the concentration of the h th metabolite in the network, and v_k ,
 132 $k = 1, \dots, n$ be the flux of the k th reaction. Every X_h must satisfy $\frac{dX_h}{dt} = \sum_{k=1}^n S_{hk}v_k$, where S_{hk} is
 133 the stoichiometric coefficient of h in the k th reaction, with the assumption that $S_{hk} < 0$ for substrates
 134 and $S_{hk} > 0$ for products. Under the assumption of steady state conditions ($\frac{dX_h}{dt} = 0$), the flux balance
 135 constraint is $Sv = 0$.

136 Typically, there are more reactions than metabolites, thus Equation $Sv = 0$ is a highly underdetermined
 137 linear system, leading to a plurality of solutions. The solution space can be restricted by imposing
 138 additional capacity constraints on the fluxes, e.g. defining the lower and upper bounds of each flux
 139 $V_k^\perp \leq v_k \leq V_k^\top$, where V_k^\perp and V_k^\top are the minimum and maximum flux rates for the k th reaction. A
 140 solution is taken through the maximization or the minimization of an objective function $Z = \sum_{k=1}^n f_k v_k$,
 141 which, under the above constraints, reduces to a convex optimization problem that can be efficiently
 142 solved with linear programming techniques.

143 When two objective functions are taken into account, an FBA problem can be formulated as a
 144 bilevel linear programming problem (e.g. for optimizing growth and product yield (Burgard et al.,
 145 2003)). This approach has been also adopted in metabolic engineering when optimizing models towards
 146 the overproduction of two metabolites simultaneously (Angione et al., 2013). Specifically, the FBA
 147 maximization problem becomes the *inner problem*, while an additional maximization problem constitutes
 148 the *outer problem*. The constraints of the outer maximization problem are the same as those of the inner
 149 problem, plus an additional constraint ensuring that the solution space is restricted to the solution of the
 150 inner problem. Formally, a bilevel maximization problem is defined as:

$$\begin{aligned}
 & \max && g^\top v \\
 & \text{such that} && \max && f^\top v \\
 & && \text{such that} && Sv = 0 \\
 & && && V_k^\perp \leq v_k \leq V_k^\top
 \end{aligned} \tag{1}$$

151 where f and g are vectors used to select the objectives. For instance, if in a two-objective problem we
 152 maximize the flux rates of the natural objective v_{k_1} (e.g. biomass production) and the synthetic objective
 153 v_{k_2} (e.g. contaminant uptake), we set $f_{k_1} = 1$ and $g_{k_2} = 1$. The solution of the bilevel problem (1) is
 154 a pair indicating the maximum natural objective (inner problem) allowed by the constraints $Sv = 0$ and
 155 $V_k^\perp \leq v_k \leq V_k^\top$, and the maximum synthetic objective allowed in the flux distribution that maximizes the
 156 natural objective. The bilevel problem can be converted to a single-level problem using the duality theory
 157 applied to the inner problem, which is replaced by additional constraints for the outer problem.

2.4 FBA ENCODING OF FOOD WEB AND INTEGRATION WITH DEGRADATION PATHWAYS

158 We introduce a method for integrating the PCBs bioaccumulation network with the FBA-based metabolic
 159 reconstruction of *P. putida*. In the following, we use the more compact notation of chemical reactions to
 160 describe our FBA encoding, omitting the translation to the matrix form given in Section 2.3.

FBA encoding. The basic idea is encoding each link $i \rightarrow j$ in the food web with a unary irreversible reaction with substrate i (the prey) and product j (the predator). Ecological compartments are thus translated into metabolites. Specifically, we derive the following set of reactions:

$$R_{FW} = \{(i, j) : i \rightarrow_{[0, c_{i \rightarrow j}]} j \mid c_{i \rightarrow j} > 0\}$$

161 where the rate of a reaction (i, j) (denoted by $r_{i,j}$) is upper bounded by the original corresponding flow rate
 162 $c_{i \rightarrow j}$. This formulation admits a space of solutions with potentially reduced (even zeroed) contaminant
 163 flows, which is required in order to reproduce the contaminant removal by the bacterial metabolism.

164 Any admissible vector of fluxes for the reactions in R_{FW} entails a food web whose groups are the
 165 metabolites occurring in R_{FW} and with contaminant flows given by $r_{i,j}$ for any group i and j . A reaction
 166 $i \rightarrow j$ having null flux indicates that prey i does not contribute to the contaminant uptake of predator j ,
 167 e.g. when biomass transfer occurs between i and j ($b_{i \rightarrow j} > 0$) but i has null contaminant concentration
 168 ($C_i = 0$).

Additionally, we consider the following set of exchange reactions for expressing the external inputs and outputs of the food web:

$$E_{FW} = \{e \rightarrow_{[0, +\infty)} \emptyset \mid e \in \{\text{Respiration, Export, Landing}\}\} \text{ and}$$

$$I_{FW} = \{\emptyset \rightarrow_r i \mid i \in \{\text{Water, Import}\} \text{ and } r = \sum_j c_{i \rightarrow j}\}$$

169 The set E_{FW} contains, for each external sink e of the food web, an unbounded export reaction from e .
 170 Similarly, the set of import reactions I_{FW} has an uptake reaction for each external source, but in this case
 171 the uptake rate is set to the sum of all flows imported through i in the contaminated network ($\sum_j c_{i \rightarrow j}$).
 172 Note that it is sufficient to constrain the import reactions in order to obtain a consistent FBA encoding of
 173 the bioaccumulation model. Indeed, by mass-balance, throughflow values are conserved by the encoding
 174 and it can be shown that *the food webs entailed by the reactions in $R_{FW} \cup E_{FW} \cup I_{FW}$ are all identical*
 175 *to the original network*, up to redistribution of external exports.

176 Finally, for a generic group i , the resulting bioconcentration C_i in the entailed network is computed
 177 as the ratio between the total contaminant outflows (as reaction fluxes) and the total biomass outflows:

$$178 \quad C_i = \frac{\sum_j r_{i,j}}{\sum_j b_{i \rightarrow j}}.$$

179 *Integration with *P. putida* metabolism.* An effective way to accomplish this task is adding a dummy
 180 metabolite \bar{x} , which serves as the interface between the encoded bioaccumulation model and the bacterial
 181 reactions. In particular, \bar{x} represents the unbounded sink for all the food web groups we aim to remediate;
 182 and the unbounded source for all the metabolites describing PCBs molecules in the *P. putida* metabolism
 183 (in our case, Biphenyl and 4-Chlorobiphenyl). Clearly, these *interface reactions* could also be bounded
 184 with arbitrary or experimentally measured limiting factors to bioremediation efficiency, as done in Section
 185 3 for evaluating different degrees of bioremediation.

186 We define the *bioremediation problem*, as that of *maximizing the amount of remediated flow*, i.e. the
 187 sum of fluxes exiting³ metabolite \bar{x} in the integrated metabolism-food web network. Formally,

$$\begin{aligned} & \max \quad \sum_{\bar{x} \rightarrow x' \in I} r_{\bar{x}, x'} \\ & \text{subject to reactions} \quad R_{FW} \cup E_{FW} \cup I_{FW} \cup I \cup R \end{aligned}$$

188 where I denotes the set of interface reactions; R is the set of reactions in the *P. putida* metabolism; and
 189 R_{FW} , E_{FW} and I_{FW} describe the encoded food web.

³ Due to the mass balance assumption of FBA, influxes could have been equivalently considered.

190 Evidently, not all integrations are ecologically and biologically plausible. In our model, we consider two
 191 bioremediation scenarios, as also shown in Figure 1:

- *Scenario 1: Bioremediation of detritus groups.* This hypothesis is based on the fact that the microbial loop, where bioremediating bacteria are assumed to naturally operate, is located at the interface between natural detritus and planktonic groups (both included in our food web). Thus, we redirect the outflows from detritus to the microbial metabolism. The same applies to the discard group, treated as a detritus in our model. The integration reactions are:

$$I_1 = \{\text{Detritus} \xrightarrow{[0,+\infty)} \bar{x}, \text{Discard} \xrightarrow{[0,+\infty)} \bar{x}, \bar{x} \xrightarrow{[0,+\infty)} \text{Biphenyl}, \bar{x} \xrightarrow{[0,+\infty)} \text{4-Chlorobiphenyl}\}$$

- *Scenario 2: Bioremediation of water compartment.* This case describes the effects of an *in situ* bioremediation process of PCBs, regarded as acting within the water compartment (an external in our model), decreasing PCBs concentrations in the whole surrounding environmental media. The integration reactions are:

$$I_2 = \{\text{Water} \xrightarrow{[0,+\infty)} \bar{x}, \bar{x} \xrightarrow{[0,+\infty)} \text{Biphenyl}, \bar{x} \xrightarrow{[0,+\infty)} \text{4-Chlorobiphenyl}\}$$

192 The integrated models have been obtained after converting PCBs flows ($\text{mg km}^{-2} \text{ yr}^{-1}$) to the flux units
 193 used in FBA ($\text{mmol h}^{-1} \text{ gDW}^{-1}$). The conversion factor is $k = 1/(m \cdot t \cdot n)$, where m is the molar mass
 194 of a PCBs molecule (Biphenyl: $154.2078 \text{ mol g}^{-1}$; 4-Chlorobiphenyl: $188.6529 \text{ mol g}^{-1}$); $t = 8760 \text{ h}$ is
 195 the number of hours per year; and n is the amount (gDW) of actively remediating *P. putida* in the unit of
 196 space (1 km^2). k can be applied to all the PCBs flows, or as a stoichiometric coefficient in the interface
 197 reactions. In our model, we set $n = 10^{-3} \text{ gDW}$, enough to import the totality of the connected PCBs
 198 flows into the *P. putida* metabolism, and to avoid numerical errors in the optimization procedure due to
 199 excessively small flux values. However, marine metagenomic data can be used to have a finer estimation
 200 of parameter n .

2.5 ECOLOGICAL NETWORK INDICES

201 In order to assess the effects of bioremediation on our contaminated food web, we combine the evaluation
 202 of bioconcentrations with the study of ecological network indices. Typically, global indices (**Kones et al.**,
 203 2009) are used to derive unique descriptors of the structure and properties of the whole ecosystem. On the
 204 other hand, indices of species centrality (**Jordán**, 2009) are typically employed for conservation purposes
 205 and give a measure of species importance in the global functioning of the ecosystem. These notions
 206 can be naturally applied to the study of our contaminated ecological network, where central species are
 207 those having a crucial role in the trophic diffusion of PCBs among other species, while global indices
 208 provide insights into the degree of ecosystem pollution. In our evaluation, we consider *Flow Betweenness*
 209 *Centrality (FBC)* (**Freeman et al.**, 1991) and *Link Density (LD)*, even if our framework can be applied to
 210 the study of arbitrary network indices.

FBC gives the topological importance of a species in maintaining the flows among other groups. The FBC of a group i , FBC_i , is defined as

$$FBC_i = \sum_{j \neq k, j \neq i, k \neq i} (\max_G c_{j \rightarrow k} - \max_{G \setminus i} c_{j \rightarrow k})$$

211 where $\max_G c_{j \rightarrow k}$ is the maximum flow between j and k in the considered food web G and $\max_{G \setminus i} c_{j \rightarrow k}$
 212 is the maximum flow between j and k in the same network without group i .

We employ LD to obtain a structural and qualitative descriptor of the network. It expresses the average number of active links (with non-null flow) per species and, ideally, from an effective bioremediation

strategy we expect a substantial breakdown of this property. It is calculated as:

$$LD = \frac{\sum_i \sum_j (c_{i \rightarrow j} > 0)}{n}$$

213 where n is the number of groups in the network.

3 RESULTS

214 The approach for the estimation of the PCBs bioaccumulation model and for the analysis of network
215 indices was implemented in R (using packages *LIM* (van Oevelen et al., 2010) and *sna* (Butts, 2008)).
216 The MATLAB-based *COBRA toolbox* (Schellenberger et al., 2011) was used for constructing and
217 analyzing our extension of the *P. putida* metabolism as well as for the reaction-based encoding and
218 integration of the food web⁴.

3.1 PCBs METABOLISM IN KT2440 AND INTERACTIONS WITH TOLUENE DEGRADATION

219 By applying bilevel FBA, the growth rate of *P. putida* remains at the maximum value (1.3975 h⁻¹) for
220 PCBs uptake rate up to 9.8 mmol h⁻¹ gDW⁻¹ (Figure 3 (a)). The maximum PCBs uptake supported by *P.*
221 *putida* is registered at 10 mmol h⁻¹ gDW⁻¹, since the rate of PCBs uptake stays constant for upper bounds
222 greater than this value. Therefore, robust growth is achieved for almost the whole range of admissible
223 PCBs uptake rates. Nevertheless, for PCBs uptake rates greater than 9.8 mmol h⁻¹ gDW⁻¹, biomass
224 production drops to the 71% of its maximum value (1 h⁻¹), indicating that the bacterium is not able to
225 support growth while degrading large amount of PCBs. Further, the addition of the PCBs bioremediation
226 pathways to the *P. putida* metabolism does not result in an increased growth rate.

227 In order to investigate the relation between growth rate and oxygen uptake, and between PCBs uptake
228 and oxygen uptake, we apply a single-level FBA analysis. In Figure 3 (b), we evaluate the optimal flux
229 of biomass and PCBs uptake rate at different levels of oxygen uptake (simulating different depths in the
230 marine environment). While the optimal PCBs uptake rate is linear with the maximum oxygen uptake
231 rate allowed, the growth rate increases quickly for low import of oxygen until 0.4 mmol h⁻¹ gDW⁻¹, and
232 then remains stable even at high oxygen uptake. The *P. putida* is able to keep a high growth rate also with
233 low oxygen, which reproduces the environmental conditions describing the proposed first bioremediation
234 scenario. The linear relationship between PCBs and oxygen uptake rates is in keeping with the fact that
235 the uptake of PCBs depends on the aerobic degradation pathway.

236 We also analyse the interdependence between the PCBs degradation pathways (introduced in this work)
237 and that of toluene (in the original reconstruction). We derive an optimality front between them by solving
238 two bilevel problems. In the first, we evaluate the maximum toluene uptake when PCBs imports are
239 favoured, while in the second problem, we consider the symmetric objectives. Both problems identify the
240 identical linear trade-off (red dashed line in Figure 3 (c)), evidencing that *P. putida* is not able to optimally
241 support multiple degradation pathways. We further perform a phenotypic phase plane (PhPP) analysis by
242 coupling the biomass production objective with varying PCBs and toluene uptake rates. In this case, we
243 seek to optimize growth on top of the configuration maximizing both degradation pathways (the sum of
244 PCBs and toluene uptakes). The PCBs-toluene tradeoff delineates two regions in the phenotypic space:
245 when the uptakes of PCBs and toluene are below the optimal front, maximum growth is achieved (100%,
246 green area in Fig. 3 (c)); and when they exceed the front, we found a reduced growth (71%, blue area).
247 Negligible regions with 90% growth (yellow points) are found at the border between the two phenotypes.
248 Specifically we observe that optimal growth is achieved for PCBs and toluene fluxes strictly below this

⁴ The extended *P. putida* model was deposited in BioModels Database (Li et al., 2010), id: MODEL1407250000. The code and the models developed in this work are available at http://www.nicolapaoletti.com/files/research/models/Frontiers_model.zip.

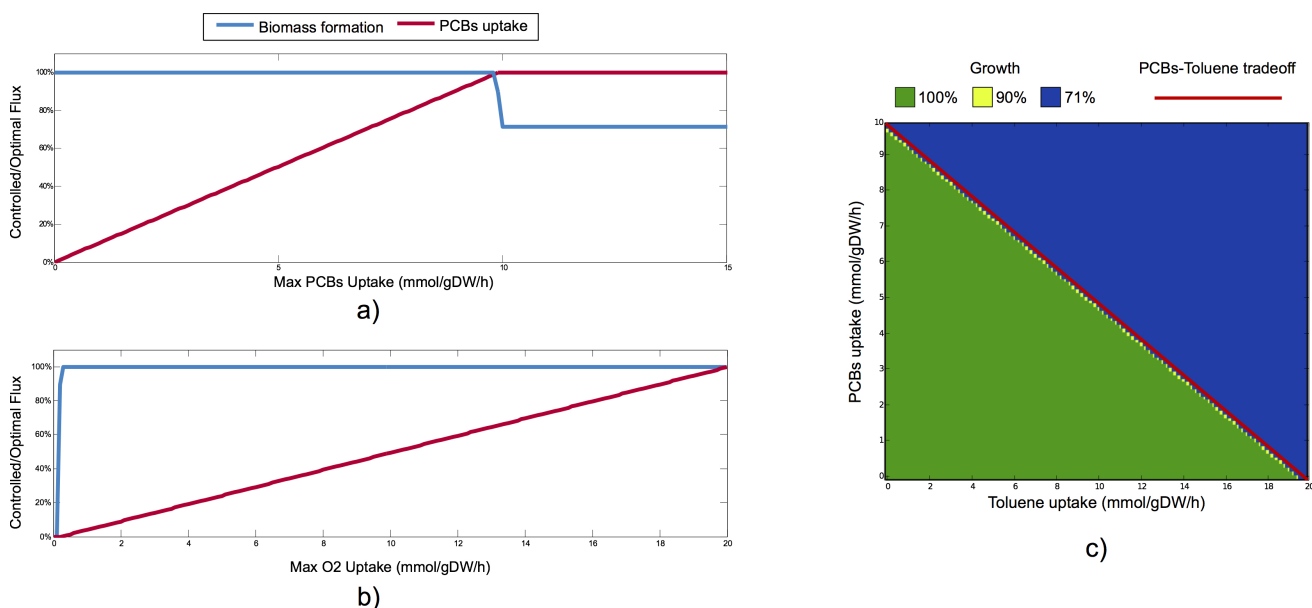


Figure 3. (a) Bilevel analysis on the *P. putida* metabolism: we study the optimal growth rates on the solution space of optimal PCBs uptake (L1), when the upper bound of the latter ranges from 0 to 15 mmol h⁻¹ gDW⁻¹. The maximum PCBs uptake rate is 10 mmol h⁻¹ gDW⁻¹, and the optimal growth rate is thus achieved for almost the whole range of PCBs uptake. (b) Single-level analysis: controlled/optimal flux of biomass and PCBs uptake rate at different oxygen levels, which in our case are determined also by different depths. The *P. putida* is able to keep a high growth rate also on low oxygen. The linear relationship between PCBs and oxygen uptake rates is in keeping with the fact that the uptake of PCBs depends on aerobic degradation. (c) Interdependence between toluene and PCBs uptake and corresponding phenotypic phase plane (PhPP). The red dashed line shows the trade-off between toluene and PCBs uptakes, obtained with a bilevel analysis of optimal toluene uptake (L2), over the configuration maximizing PCBs uptake (L1), by limiting the latter from 0 to 10 mmol h⁻¹ gDW⁻¹. The symmetric bilevel problem (with toluene limited from 0 to 20 mmol h⁻¹ gDW⁻¹) gives the same linear front. This tradeoff delineates two phenotypes in the PhPP analysis (L2: biomass, L1: toluene+PCBs uptakes): in the lower half (green region), we have optimal growth; in the upper half (blue region), growth is limited to the 71%.

249 trade-off, implying that reduced growth occurs also at high uptake values (PCBs flux > 9.8 mmol h⁻¹
 250 gDW⁻¹, toluene flux > 19.7 mmol h⁻¹ gDW⁻¹), as also seen for the PCBs case in plot (a). It follows
 251 that, apart from extreme uptake values, the *P. putida* robustly gives optimal growth yields even in the
 252 strain designs targeted to the maximization of multiple degradation pathways.

3.2 BIOREMEDIATION EFFECTS ON BIOACCUMULATION AND SPECIES CENTRALITY

253 We analyse the integrated models obtained by applying the two scenarios introduced in Section 2.4.
 254 In Scenario 1, microbial degradation pathways reduce contaminant concentrations through outflows
 255 from natural detritus and fishing discards (functional groups 38 and 39, trophic level=1), simulating a
 256 bioremediation at the level of the microbial loop. In Scenario 2, PCBs bioremediation is assumed to act
 257 in the water compartment by reducing simultaneously all the PCBs uptakes in each functional group.
 258 The following results are obtained by solving the bioremediation problem (Sect. 2.4) and computing
 259 bioconcentrations and network indices on the resulting (the entailed) bioaccumulation networks.

260 In Figure 4, we illustrate in a circular layout the PCBs bioaccumulation networks of a business-as-
 261 usual case without bioremediation, hereafter called *Scenario 0* (plot (a)), and of the above two scenarios
 262 when no limits to the bioremediation efficiency are imposed (plot (b) and (c)). Fig. 4 depicts only the
 263 contaminant flows mediated by feeding links. Plot (a) highlights that in Scenario 0, contaminant diffusion
 264 throughout the food web is driven by a dense network of trophic connections, each of them carrying a
 265 non-null PCBs flow.

266 In Scenario 1 (plot (b)), we clearly notice a simpler pattern of PCBs contamination among functional
267 groups, due to a considerable reduction of feeding links active in the transport of PCBs. Specifically,
268 the redirection of outflows from detritus and discard out of the food web causes the inactivation of
269 several PCBs flows, and subsequent presence of groups with null PCBs concentration. Therefore, these
270 groups (not plotted) are disconnected from the bioaccumulation network but still active in the biomass
271 network. They include detritus (38) and discard (39); detritivores (6,7,8); group 30, which totally feeds
272 on planktonic groups; and groups feeding on those so far mentioned (33, 34, 35). Other variations
273 are detectable in groups 5, 27 and 28 (detritivores and planktivores) that no longer acquire PCBs
274 from food. Finally, we can observe that groups 12 and 27 gain in this scenario a central role in the
275 contaminant diffusion, becoming the preferential source of most of their predators, while in Scenario 0
276 their contribution appears less relevant.

277 The bioaccumulation network under Scenario 2 (plot (c)) exhibits a similar structure to Scenario 1.
278 Detritus groups (38,39) and detritivores (6,7,8) are no longer connected to the rest of the food web,
279 showing that bioremediation of the water compartment tends to disrupt the pathways of contaminant
280 uptake at the lowest trophic levels. Another similarity is the promotion of group 12 as a central node in
281 the acquisition of PCBs by its predators. On the other hand, group 27 has no outgoing PCBs flows, while
282 in plot (b) the opposite situation (no inflows) is observed for the same group. In general, we notice a lower
283 number of active links with respect to Scenario 1, especially in species at higher trophic levels.

284 Another kind of analysis enabled by our framework is the study of the networks obtained by solving
285 the bioremediation problem at increasing efficiencies, limiting the amount of PCBs flow allowed into the
286 bacterial metabolism. In both scenarios, we analyse the variations in PCBs bioconcentrations (Fig. 5 (a)
287 and (b)) and in the topological importance of functional groups, measured with the FBC index introduced
288 in Section 2.5 (Fig. 5 (c) and (d)). We report a difference between the maximum remediated PCBs flows
289 in the two scenarios ($4258 \text{ mg km}^{-2} \text{ y}^{-1}$ and $3312 \text{ mg km}^{-2} \text{ y}^{-1}$, respectively), which mainly depends
290 on the structure of the network. Applying the conversion factor in Section 2.4, the maximum remediated
291 flow in Scenario 1 corresponds to a PCBs uptake rate of $3.15 \text{ mmol h}^{-1} \text{ gDW}^{-1}$ (31.5% of the maximum
292 uptake), while in Scenario 2 to $2.45 \text{ mmol h}^{-1} \text{ gDW}^{-1}$ (24.5% of the maximum uptake).

293 As regards Scenario 1, no remarkable reductions in bioconcentrations are observed in the entire food
294 web (see plot (a)), apart from the natural detritus and the discard groups, whose PCBs values are zeroed at
295 the 89% and 16%, respectively, of the maximum bioremediation efficiency. We register only minor drops
296 in a number of groups at TL 4 (14, 16, 23, 24) and in group 37 (feeding on discard). This tendency is also
297 visible in the sum of PCBs, which is practically constant.

298 On the other hand, Scenario 2 gives a considerable decrease in the bioconcentrations of all groups
299 (plot (b)). This is explained by the fact that the estimated uptakes from water constitute an important
300 fraction of imported contaminant, whose degradation also mitigates, indirectly, uptakes from food. The
301 only exceptions are natural detritus and discard (38, 39) which have null PCBs flow from water (see Table
302 1); and groups 26 and 35 where according to our estimation, water imports are the least relevant external
303 uptakes. In general, the sum of PCBs concentrations shows a constant and gradual decreasing trend,
304 even though steeper reductions are observable at low values of microbial degradation (2% of maximum
305 efficiency gives a 17% drop in the sum of PCBs), and at about the 34% of the maximum bioremediation
306 (leading to the 48% reduction of the initial total PCBs).

307 In Scenario 1, the analysis of the FBC index (plot (c)) highlights the topological importance of natural
308 detritus in the bioaccumulation network, which derives from the fact that every group in the food web
309 contributes (via natural death and unassimilated food) to its contaminant uptake. Indeed, this group
310 maintains its central role up to the 89% of bioremediation efficiency. After this point, a structural
311 disruption occurs, related to the detritus becoming disconnected from the network (i.e. no incident flows).
312 This leads to cascade effects also in the centrality of groups 13, 15, 16, 19 and 32. Apart from this
313 case, FBC exhibits quite a robust pattern, showing a number of groups (2, 21, 22, 25) with unchanged
314 centralities regardless of the amount of bioremediated flux. This structural robustness is evidenced also

315 by the link density values, indicating that, globally, the number of links active in the PCBs diffusion are
316 relatively constant.

317 On the contrary, Scenario 2 (plot (d)) produces prominent changes in the centrality of most species.
318 Here, natural detritus loses its dominant role in the network at the 10% of maximum bioremediation.
319 Moreover, at the 34% efficiency, we observe a sudden fall in the FBC of group 24, as also registered
320 on its bioconcentration values (see plot (b)). Only functional groups 2 and 25 show robust topological
321 importance, in agreement with Scenario 1. The evolution of the link density index also evidences the high
322 sensitivity of the network structure. Indeed, the index reaches an average of 3.1429 active links per group,
323 36% lower than the initial value.

4 DISCUSSION

324 Recent biotechnological advances and novel discovery tools in marine metagenomics are paving the way
325 for new integrated solutions in environmental bioengineering, turning empirical hypotheses into practical
326 methods. In this context, we presented a computational framework for the analysis of contaminated
327 ecosystems and for the evaluation of different hypothetical bioremediation scenarios. We considered the
328 case of PCBs bioaccumulation in the Adriatic food web and PCBs degradation microbially mediated by
329 *Pseudomonas putida*. Our framework is based on a range of multi-scale analyses obtained by combining
330 well-established methods in ecological modelling (Linear Inverse Modelling and Ecological Network
331 Analysis) and Systems Biology (Flux Balance Analysis). We showed how to derive optimal remediation
332 strategies that yield the highest decrease of bioaccumulation phenomena in species. In addition, more
333 realistic scenarios can be reproduced that take into account environmental limiting factors influencing the
334 potential of natural or synthetically designed microbial pathways.

335 Our computational experiments indicated that *P. putida* metabolically supports well the degradation
336 of PCBs, and that a substantial drop of PCBs concentration in Adriatic species is achieved with
337 comprehensive bioremediation strategies (e.g. Scenario 2: bioremediation of water compartments),
338 while natural bioremediation (e.g. Scenario 1: bioremediation of detritus group) proved to be less
339 effective. Results also highlight how remediation patterns vary among species in function of their
340 feeding relationships. The study of ecological network indices allowed the evaluation of emerging global
341 ecosystem properties under different bioremediation scenarios and degradation efficiencies.

342 To the best of our knowledge, this is the first computational method linking genome-scale
343 reconstructions of bacterial metabolism with food web bioaccumulation models for designing and
344 analysing bioremediation strategies. Approaches based on high dimensional omics data and network
345 inference methods (Williams et al., 2011; Perkins et al., 2011) have been proposed for predicting the
346 exposure of organisms to contaminated sites and for reconstructing adverse outcome pathways (Ankley
347 et al., 2010). From the experimental side, Kupryianchik et al. (2013) were the first to study how in situ
348 sediment treatment reduces bioaccumulation at different trophic levels in aquatic food chains.

349 In this work we wanted to stress a different view on marine ecosystems, regarding them not just
350 as ensembles of macro-species, but as complex multiscale networks linking classical food webs and
351 microbial communities, towards a new perspective of “eco-metabolic” networks. We believe that bringing
352 the study of microbial metabolic activity into the field of ecotoxicological modelling can highlight
353 bottlenecks and advantages of different bioremediation approaches and shed light on the ecological role of
354 marine microbial life. Furthermore, PCBs degrading bacteria live in communities structurally organized in
355 biofilms (Abraham et al., 2002), where genetic events like recombination, conjunction and gene transfer
356 (Dahlberg et al., 1998) can naturally lead to new metabolic pathways of pollutant degradation. In this
357 perspective, our framework could be extended from single organism models to the bioengineering of
358 bacterial consortia, e.g. following (Brenner et al., 2008; Klitgord and Segrè, 2010), where natural
359 genetic interactions can be explored and synthetically optimized for different persistent contaminants.

REFERENCES

- 360 Abraham, W.-R., Nogales, B., Golyshin, P. N., Pieper, D. H., and Timmis, K. N. (2002), Polychlorinated
361 biphenyl-degrading microbial communities in soils and sediments, *Current Opinion in Microbiology*,
362 5, 3, 246–253
- 363 Angione, C., Carapezza, G., Costanza, J., Liò, P., and Nicosia, G. (2013), Pareto optimality in organelle
364 energy metabolism analysis, *IEEE/ACM Transactions on Computational Biology and Bioinformatics*
365 (*TCBB*), 10, 4, 1032–1044
- 366 Ankley, G. T., Bennett, R. S., Erickson, R. J., Hoff, D. J., Hornung, M. W., Johnson, R. D., et al.
367 (2010), Adverse outcome pathways: a conceptual framework to support ecotoxicology research and
368 risk assessment, *Environmental Toxicology and Chemistry*, 29, 3, 730–741
- 369 Bayarri, S., Baldassarri, L. T., Iacovella, N., Ferrara, F., and Domenico, A. d. (2001), Pcds, pcdfs, pcbs
370 and dde in edible marine species from the adriatic sea, *Chemosphere*, 43, 4, 601–610
- 371 Bedard, D. L. and Quensen III, J. F. (1995), Microbial reductive dechlorination of polychlorinated
372 biphenyls, *Microbial transformation and degradation of toxic organic chemicals*, 127–216
- 373 Brenner, K., You, L., and Arnold, F. H. (2008), Engineering microbial consortia: a new frontier in
374 synthetic biology, *Trends in biotechnology*, 26, 9, 483–489
- 375 Brown Jr, J. F., Bedard, D. L., Brennan, M. J., Carnahan, J. C., Feng, H., and Wagner, R. E. (1987),
376 Polychlorinated biphenyl dechlorination in aquatic sediments, *Science*, 236, 4802, 709–712
- 377 Burgard, A. P., Pharkya, P., and Maranas, C. D. (2003), Optknock: a bilevel programming framework
378 for identifying gene knockout strategies for microbial strain optimization, *Biotechnology and*
379 *bioengineering*, 84, 6, 647–657
- 380 Butts, C. T. (2008), Social network analysis with sna, *Journal of Statistical Software*, 24, 6, 1–51
- 381 Christensen, V. and Walters, C. (2004), Ecopath with Ecosim: methods, capabilities and limitations,
382 *Ecological modelling*, 172, 2, 109–139
- 383 Coll, M., Piroddi, C., Steenbeek, J., Kaschner, K., Lasram, F. B. R., Aguzzi, J., et al. (2010), The
384 biodiversity of the mediterranean sea: estimates, patterns, and threats, *PloS one*, 5, 8, e11842
- 385 Coll, M., Santojanni, A., Palomera, I., Tudela, S., and Arneri, E. (2007), An ecological model of the
386 northern and central adriatic sea: Analysis of ecosystem structure and fishing impacts, *Journal of*
387 *Marine Systems*, 67, 1, 119–154
- 388 Corsolini, S., Aurigi, S., and Focardi, S. (2000), Presence of polychlorobiphenyls (pcbs) and coplanar
389 congeners in the tissues of the mediterranean loggerhead turtle caretta caretta, *Marine Pollution*
390 *Bulletin*, 40, 11, 952–960
- 391 Dahlberg, C., Bergström, M., and Hermansson, M. (1998), In situ detection of high levels of horizontal
392 plasmid transfer in marine bacterial communities, *Applied and environmental microbiology*, 64, 7,
393 2670–2675
- 394 Danovaro, R., Corinaldesi, C., D’Onghia, G., Galil, B., Gambi, C., Gooday, A. J., et al. (2010), Deep-sea
395 biodiversity in the mediterranean sea: The known, the unknown, and the unknowable, *PLoS One*, 5, 8,
396 e11832
- 397 Fava, F., Zanaroli, G., and Young, L. (2003), Microbial reductive dechlorination of pre-existing pcbs and
398 spiked 2, 3, 4, 5, 6-pentachlorobiphenyl in anaerobic slurries of a contaminated sediment of venice
399 lagoon (italy), *FEMS microbiology ecology*, 44, 3, 309–318
- 400 Fenchel, T. (2008), The microbial loop–25 years later, *Journal of Experimental Marine Biology and*
401 *Ecology*, 366, 1, 99–103
- 402 Freeman, L. C., Borgatti, S. P., and White, D. R. (1991), Centrality in valued graphs: A measure of
403 betweenness based on network flow, *Social networks*, 13, 2, 141–154
- 404 Furukawa, K. (2000), Biochemical and genetic bases of microbial degradation of polychlorinated
405 biphenyls (pcbs)., *The Journal of general and applied microbiology*, 46, 6, 283–296
- 406 Furukawa, K., Hirose, J., Suyama, A., Zaiki, T., and Hayashida, S. (1993), Gene components responsible
407 for discrete substrate specificity in the metabolism of biphenyl (bph operon) and toluene (tod operon).,
408 *Journal of bacteriology*, 175, 16, 5224–5232
- 409 Furukawa, K. and Miyazaki, T. (1986), Cloning of a gene cluster encoding biphenyl and chlorobiphenyl
410 degradation in pseudomonas pseudoalcaligenes., *Journal of bacteriology*, 166, 2, 392–398

- 411 Garcia-Valdes, E., Cozar, E., Rotger, R., Lalucat, J., and Ursing, J. (1988), New naphthalene-degrading
412 marine pseudomonas strains., *Applied and environmental microbiology*, 54, 10, 2478–2485
- 413 Hendriks, A. J., van der Linde, A., Cornelissen, G., and Sijm, D. T. (2001), The power of size. 1.
414 rate constants and equilibrium ratios for accumulation of organic substances related to octanol-water
415 partition ratio and species weight, *Environmental toxicology and chemistry*, 20, 7, 1399–1420
- 416 Jordán, F. (2009), Keystone species and food webs, *Philosophical Transactions of the Royal Society B:*
417 *Biological Sciences*, 364, 1524, 1733–1741
- 418 Klitgord, N. and Segrè, D. (2010), Environments that induce synthetic microbial ecosystems, *PLoS*
419 *computational biology*, 6, 11, e1001002
- 420 Kones, J. K., Soetaert, K., van Oevelen, D., and Owino, J. O. (2009), Are network indices robust indicators
421 of food web functioning? a monte carlo approach, *Ecological Modelling*, 220, 3, 370–382
- 422 Krzywinski, M., Schein, J., Birol, I., Connors, J., Gascoyne, R., Horsman, D., et al. (2009), Circos: an
423 information aesthetic for comparative genomics, *Genome research*, 19, 9, 1639–1645
- 424 Kupryianchuk, D., Rakowska, M., Roessink, I., Reichman, E., Grotenhuis, J., and Koelmans, A. (2013),
425 In situ treatment with activated carbon reduces bioaccumulation in aquatic food chains, *Environmental*
426 *science & technology*, 47, 9, 4563–4571
- 427 Laender, F. D., Oevelen, D. V., Middelburg, J. J., and Soetaert, K. (2009), Incorporating ecological data
428 and associated uncertainty in bioaccumulation modeling: methodology development and case study,
429 *Environmental science & technology*, 43, 7, 2620–2626
- 430 Li, C., Donizelli, M., Rodriguez, N., Dharuri, H., Endler, L., Chelliah, V., et al. (2010), Biomodels
431 database: An enhanced, curated and annotated resource for published quantitative kinetic models, *BMC*
432 *systems biology*, 4, 1, 92
- 433 Lovley, D. R. (2003), Cleaning up with genomics: applying molecular biology to bioremediation, *Nature*
434 *Reviews Microbiology*, 1, 1, 35–44
- 435 Marcotrigiano, G. and Storelli, M. (2003), Heavy metal, polychlorinated biphenyl and organochlorine
436 pesticide residues in marine organisms: risk evaluation for consumers, *Veterinary research*
437 *communications*, 27, 1, 183–195
- 438 Nogales, J., Palsson, B. Ø., and Thiele, I. (2008), A genome-scale metabolic reconstruction of
439 pseudomonas putida kt2440: ijn746 as a cell factory, *BMC systems biology*, 2, 1, 79
- 440 Orth, J., Thiele, I., and Palsson, B. (2010), What is flux balance analysis?, *Nature biotechnology*, 28, 3,
441 245–248
- 442 Perkins, E. J., Chipman, J. K., Edwards, S., Habib, T., Falciani, F., Taylor, R., et al. (2011), Reverse
443 engineering adverse outcome pathways, *Environmental Toxicology and Chemistry*, 30, 1, 22–38
- 444 Perugini, M., Cavaliere, M., Giammarino, A., Mazzone, P., Olivieri, V., and Amorena, M. (2004), Levels
445 of polychlorinated biphenyls and organochlorine pesticides in some edible marine organisms from the
446 Central Adriatic Sea, *Chemosphere*, 57, 5, 391–400
- 447 Pieper, D. H. and Reineke, W. (2000), Engineering bacteria for bioremediation, *Current Opinion in*
448 *Biotechnology*, 11, 3, 262–270
- 449 Sagratini, G., Buccioni, M., Ciccarelli, C., Conti, P., Cristalli, G., Giardina, D., et al. (2008), Levels of
450 polychlorinated biphenyls in fish and shellfish from the adriatic sea, *Food Additives and Contaminants*,
451 1, 1, 69–77
- 452 Schellenberger, J., Que, R., Fleming, R. M., Thiele, I., Orth, J. D., Feist, A. M., et al. (2011), Quantitative
453 prediction of cellular metabolism with constraint-based models: the cobra toolbox v2. 0, *Nature*
454 *protocols*, 6, 9, 1290–1307
- 455 Storelli, M., Barone, G., and Marcotrigiano, G. (2007), Polychlorinated biphenyls and other chlorinated
456 organic contaminants in the tissues of mediterranean loggerhead turtle caretta caretta, *Science of the*
457 *Total Environment*, 373, 2, 456–463
- 458 van Oevelen, D., Van den Meersche, K., Meysman, F., Soetaert, K., Middelburg, J., and Vézina, A.
459 (2010), Quantifying food web flows using linear inverse models, *Ecosystems*, 13, 1, 32–45
- 460 Williams, T. D., Turan, N., Diab, A. M., Wu, H., Mackenzie, C., Bartie, K. L., et al. (2011), Towards a
461 system level understanding of non-model organisms sampled from the environment: a network biology
462 approach, *PLoS computational biology*, 7, 8, e1002126

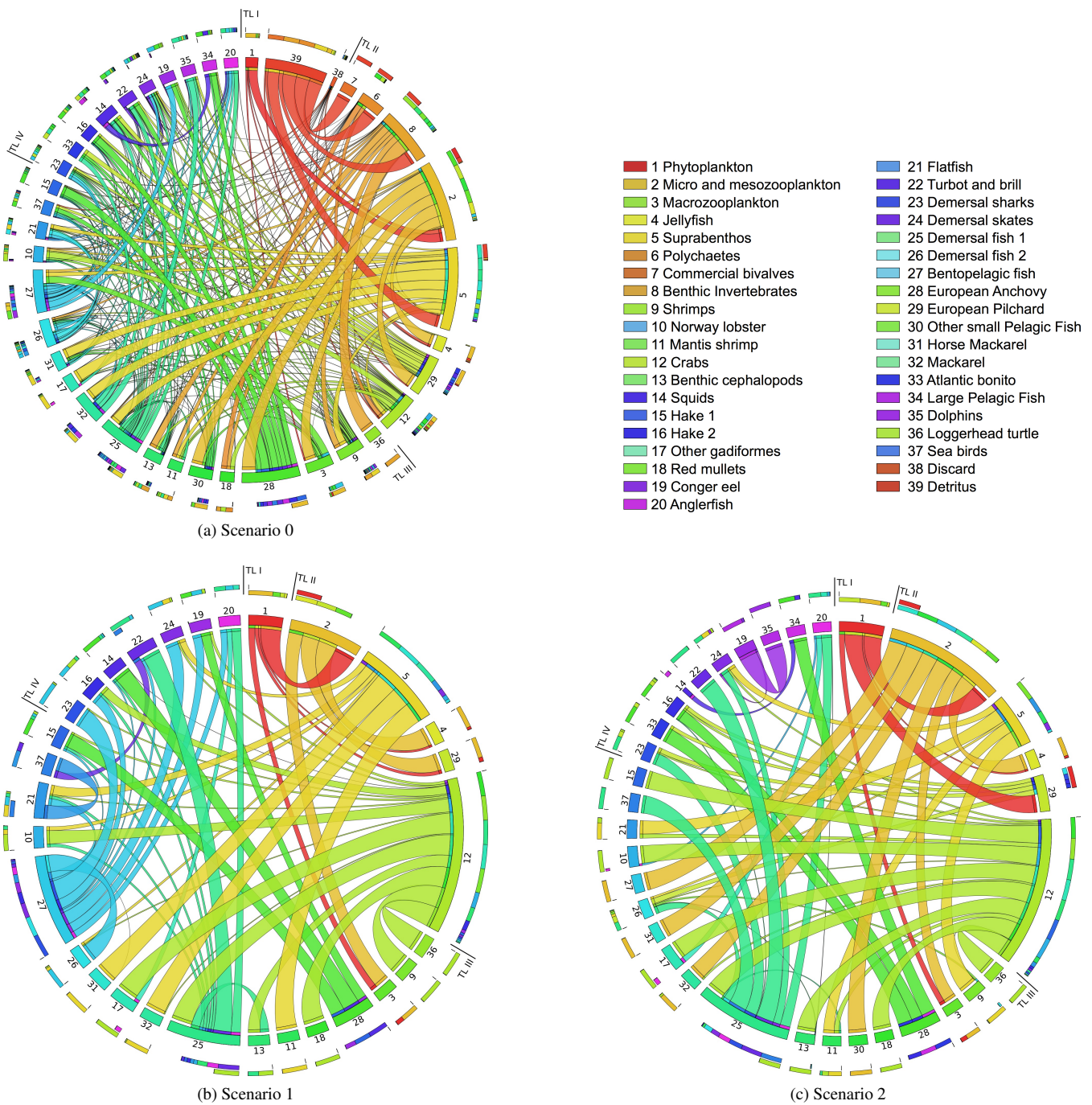


Figure 4. Circular plot of the Adriatic food web in the three cases considered: PCBs bioaccumulation network without bioremediation (Scenario 0); at maximum bioremediation efficiency for the natural bioremediation acting on detritus and discard (Scenario 1); and the in-situ bioremediation acting on the water compartment (Scenario 2). Functional groups are located clock-wise in ascending trophic level order. Ribbons represent feeding links carrying PCBs flows. Each ribbon takes the same color as its source node (the prey), and thickness is proportional to the contribution of the source in the diet of the target node (the predator). In each group, the outmost stacked bars summarize its diet composition and its contribution to predators' diet. External and flows to detritus groups are not displayed. The top-right table lists report the functional groups of the Adriatic food web and their ID numbers. Images has been obtained by using Krzywinski et al. (2009).

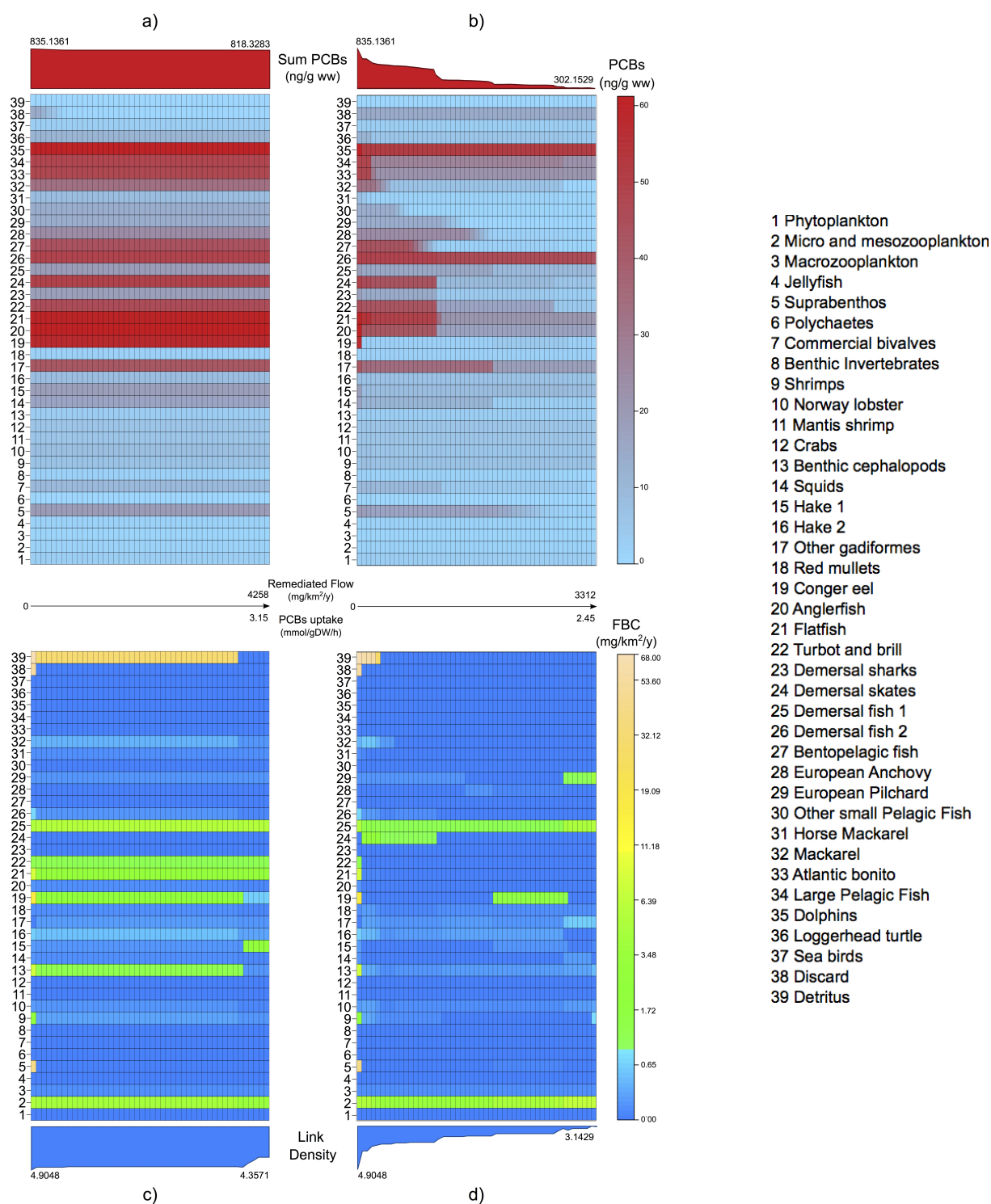
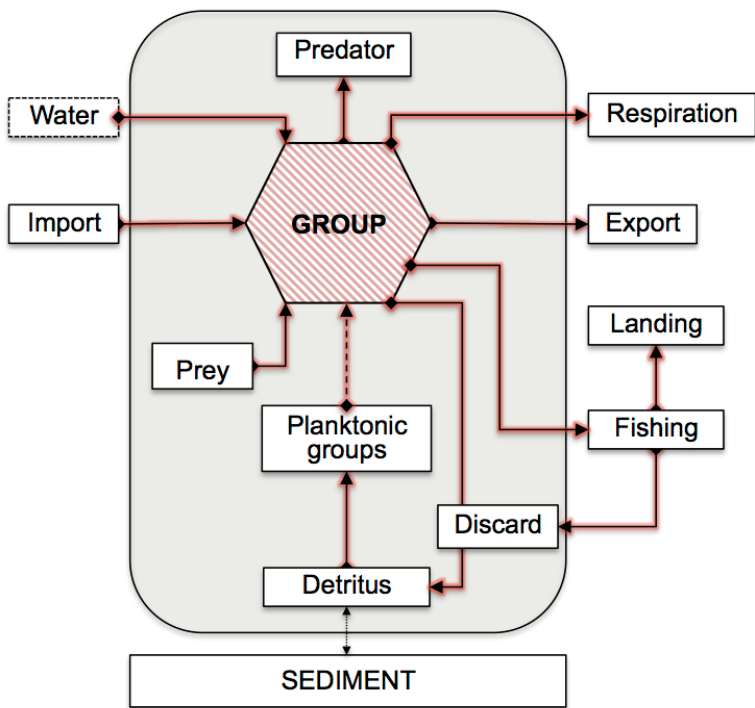
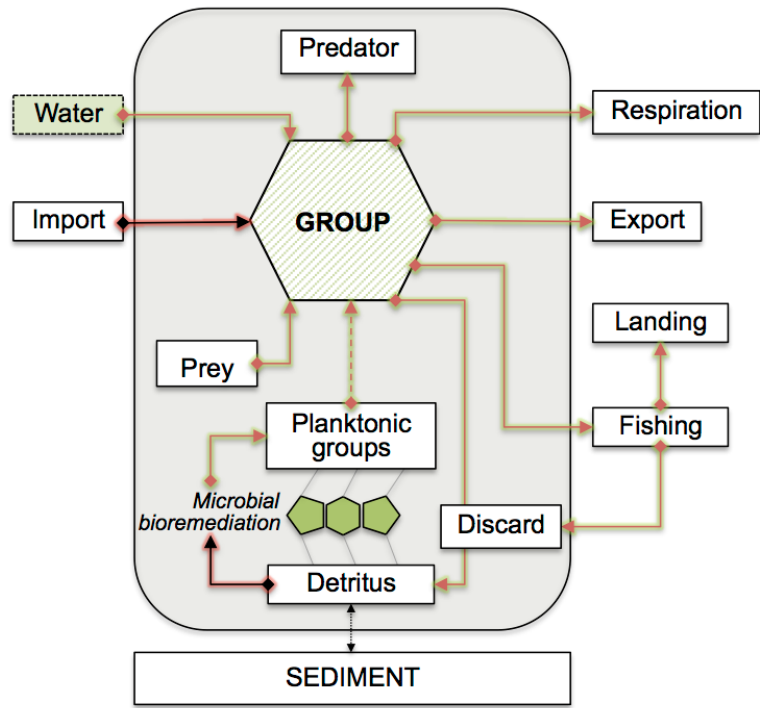


Figure 5. Levelplots of PCBs concentrations (a, b) and flow betweenness centralities (c,d) in Adriatic species (y-axis) at increasing amounts of contaminant removed by bacterial uptake (x-axis) in the natural (a,c) and in-situ (b,d) bioremediation scenarios. In the middle, the final amount of remediated flow and the corresponding PCBs uptake are reported for the two scenarios. Plots on the top of (a) and (b) show the evolution of the sum of PCBs in the food web at increasing degrees of bioremediation. Plots on the bottom of (c) and (d) show the effects of bioremediation in the link density of the bioaccumulation network.

Figure 1.TIFF



a)



b)

Figure 2.TIFF

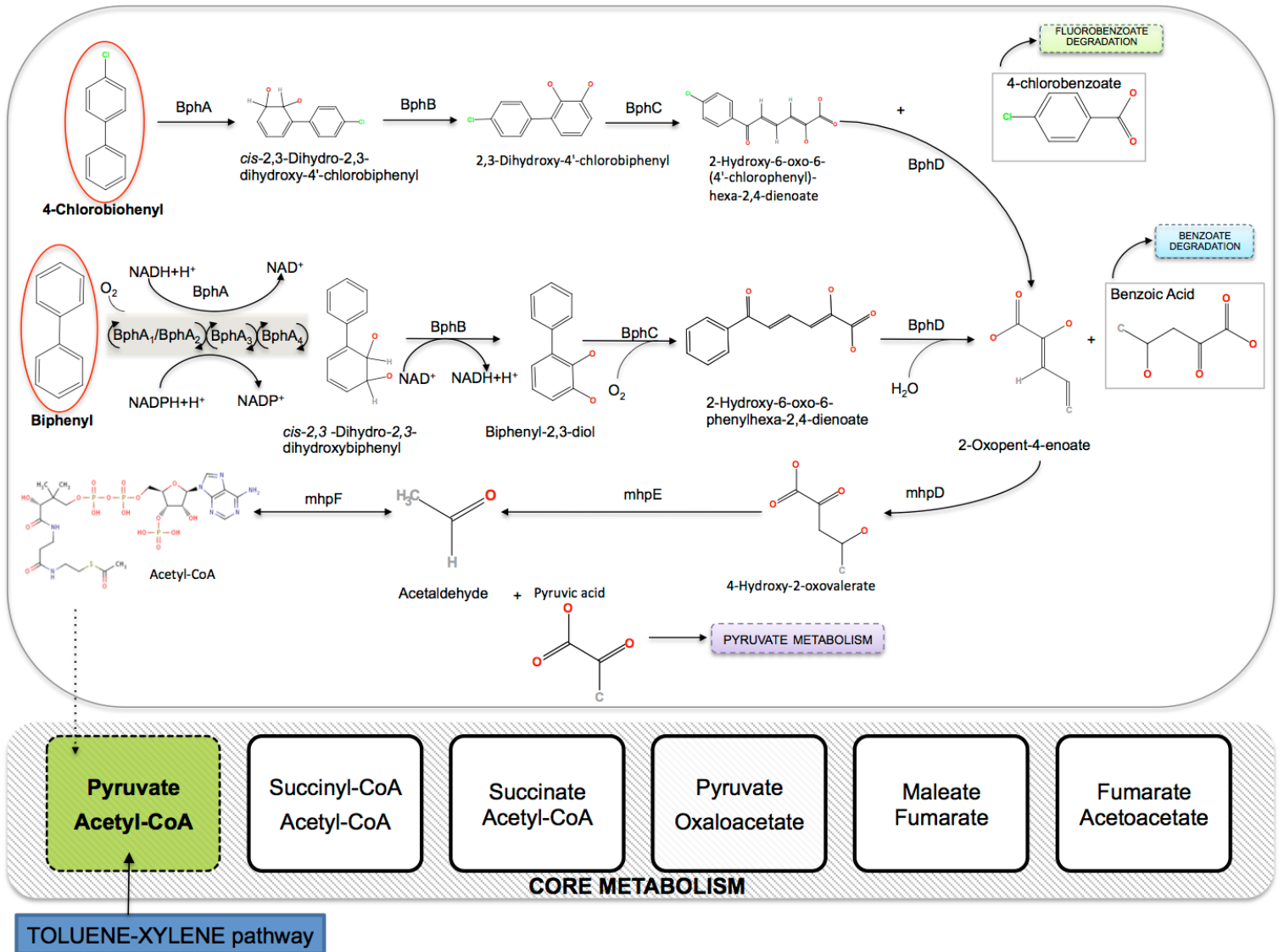


Figure 3.TIFF

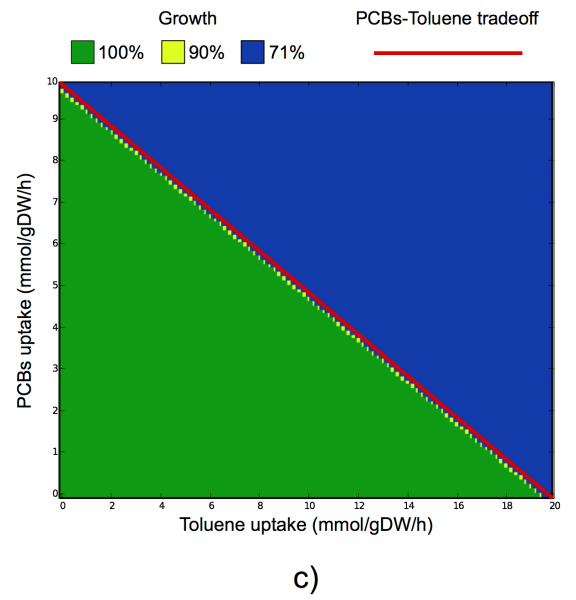
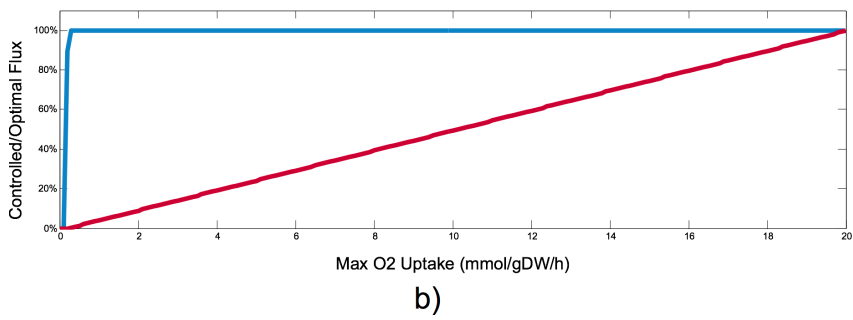
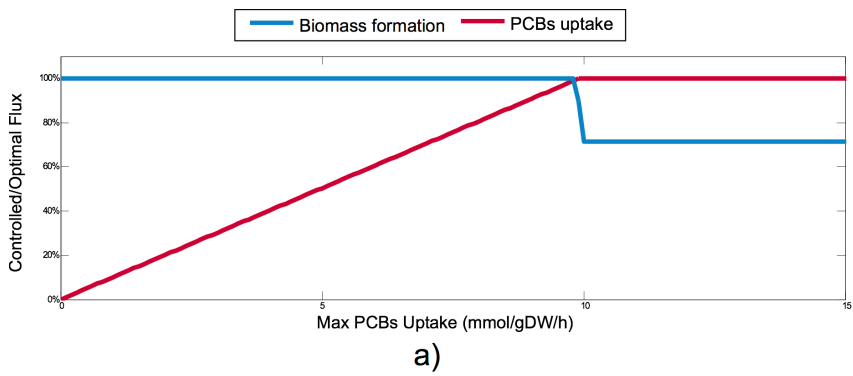


Figure 4.TIFF












- | | |
|---|--|
|  1 Phytoplankton |  21 Flatfish |
|  2 Micro and mesozooplankton |  22 Turbot and brill |
|  3 Macrozooplankton |  23 Demersal sharks |
|  4 Jellyfish |  24 Demersal skates |
|  5 Suprabenthos |  25 Demersal fish 1 |
|  6 Polychaetes |  26 Demersal fish 2 |
|  7 Commercial bivalves |  27 Bentopelagic fish |
|  8 Benthic Invertebrates |  28 European Anchovy |
|  9 Shrimps |  29 European Pilchard |
|  10 Norway lobster |  30 Other small Pelagic Fish |
|  11 Mantis shrimp |  31 Horse Mackerel |
|  12 Crabs |  32 Mackerel |
|  13 Benthic cephalopods |  33 Atlantic bonito |
|  14 Squids |  34 Large Pelagic Fish |
|  15 Hake 1 |  35 Dolphins |
|  16 Hake 2 |  36 Loggerhead turtle |
|  17 Other gadiformes |  37 Sea birds |
|  18 Red mullets |  38 Discard |
|  19 Conger eel |  39 Detritus |
|  20 Anglerfish | |

Figure 5.TIFF

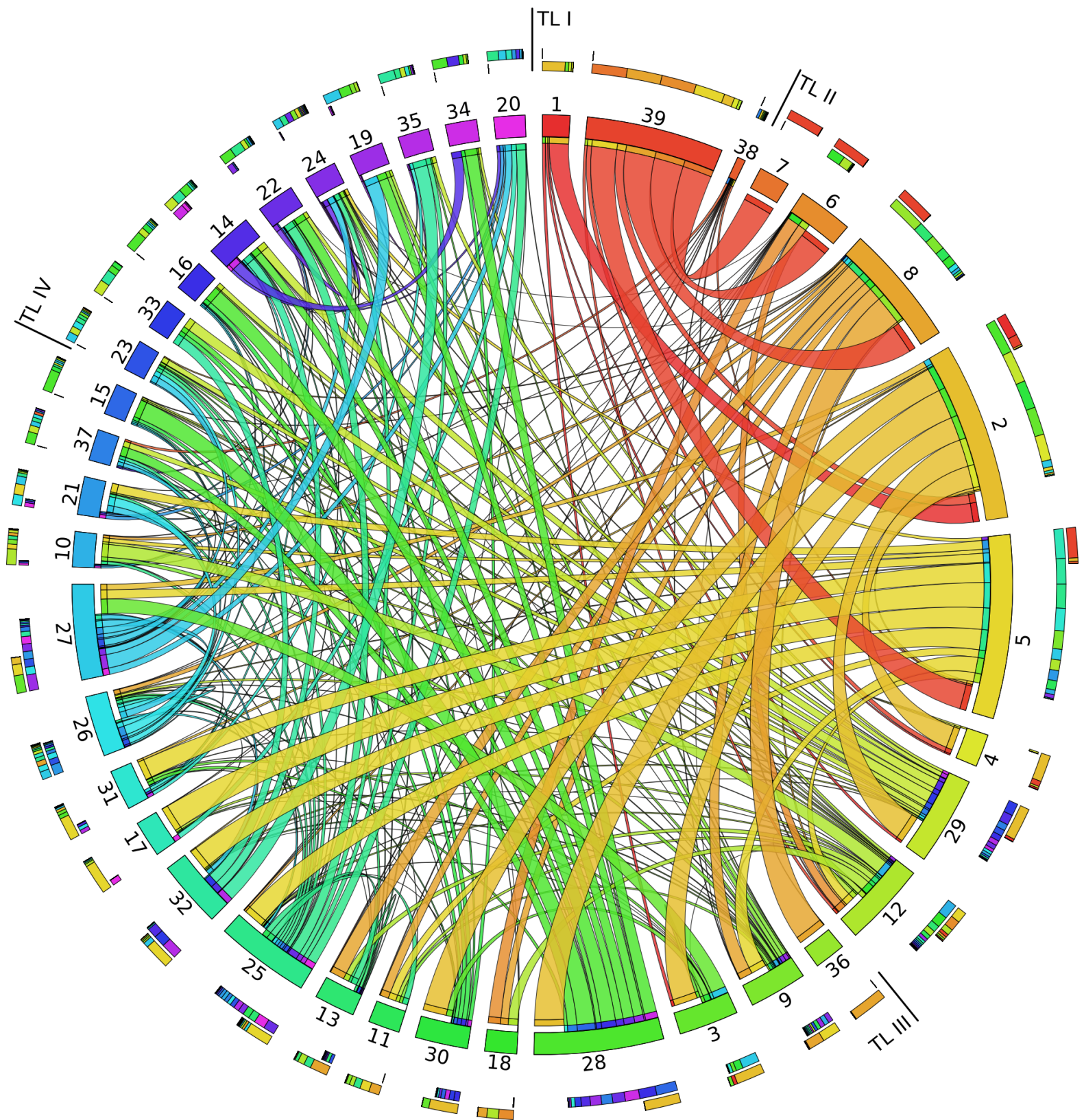


Figure 6.TIFF

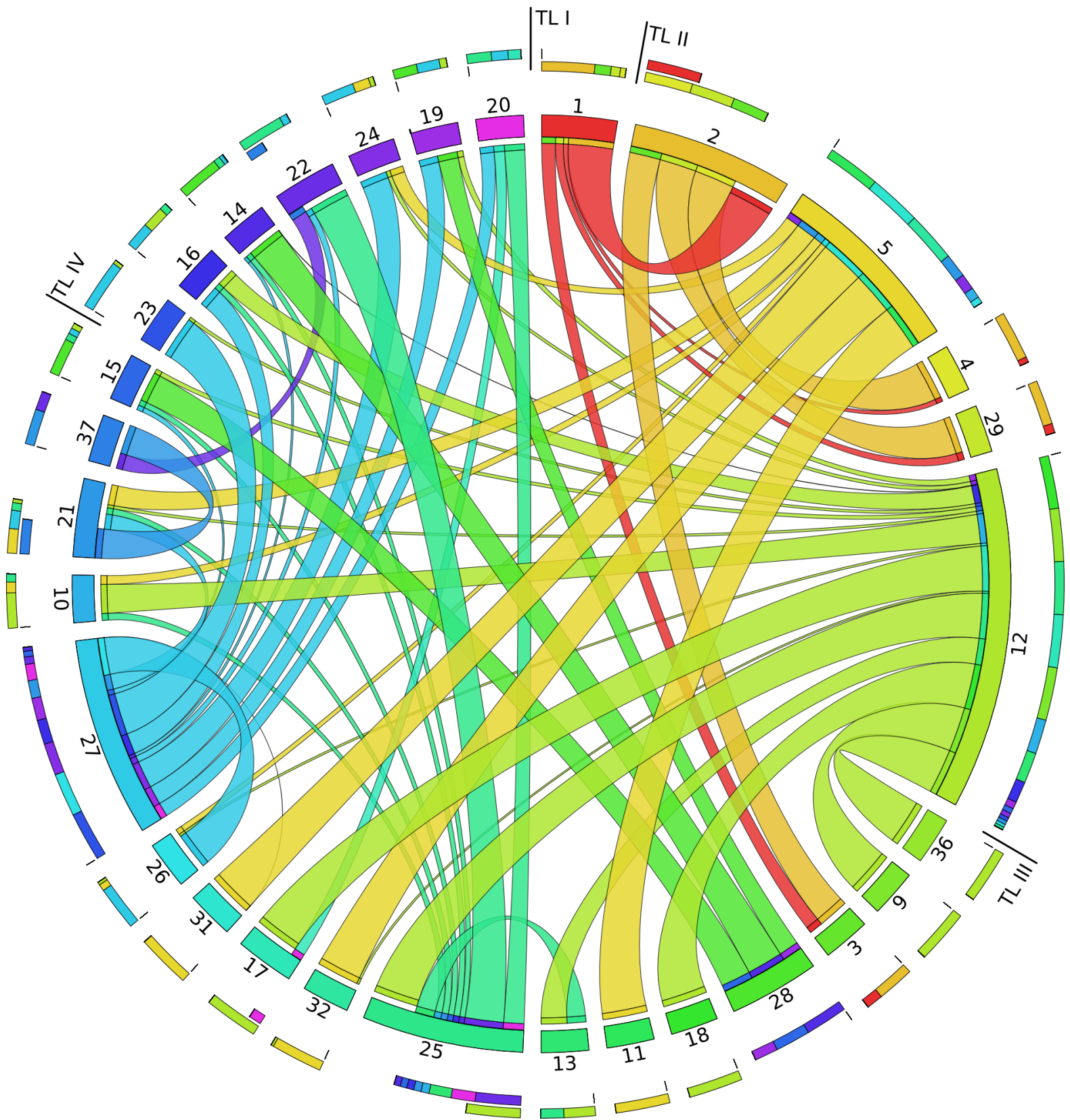
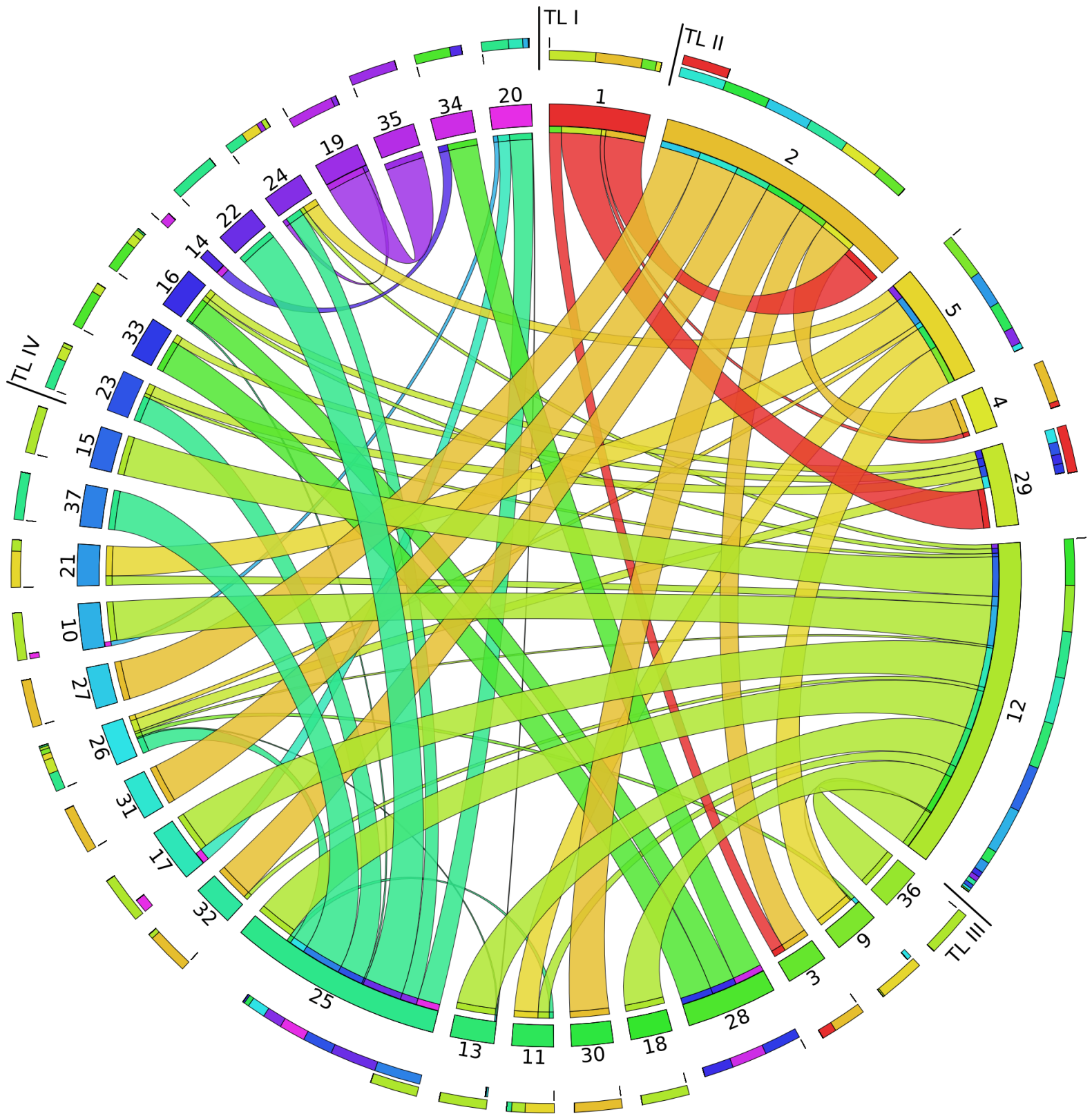
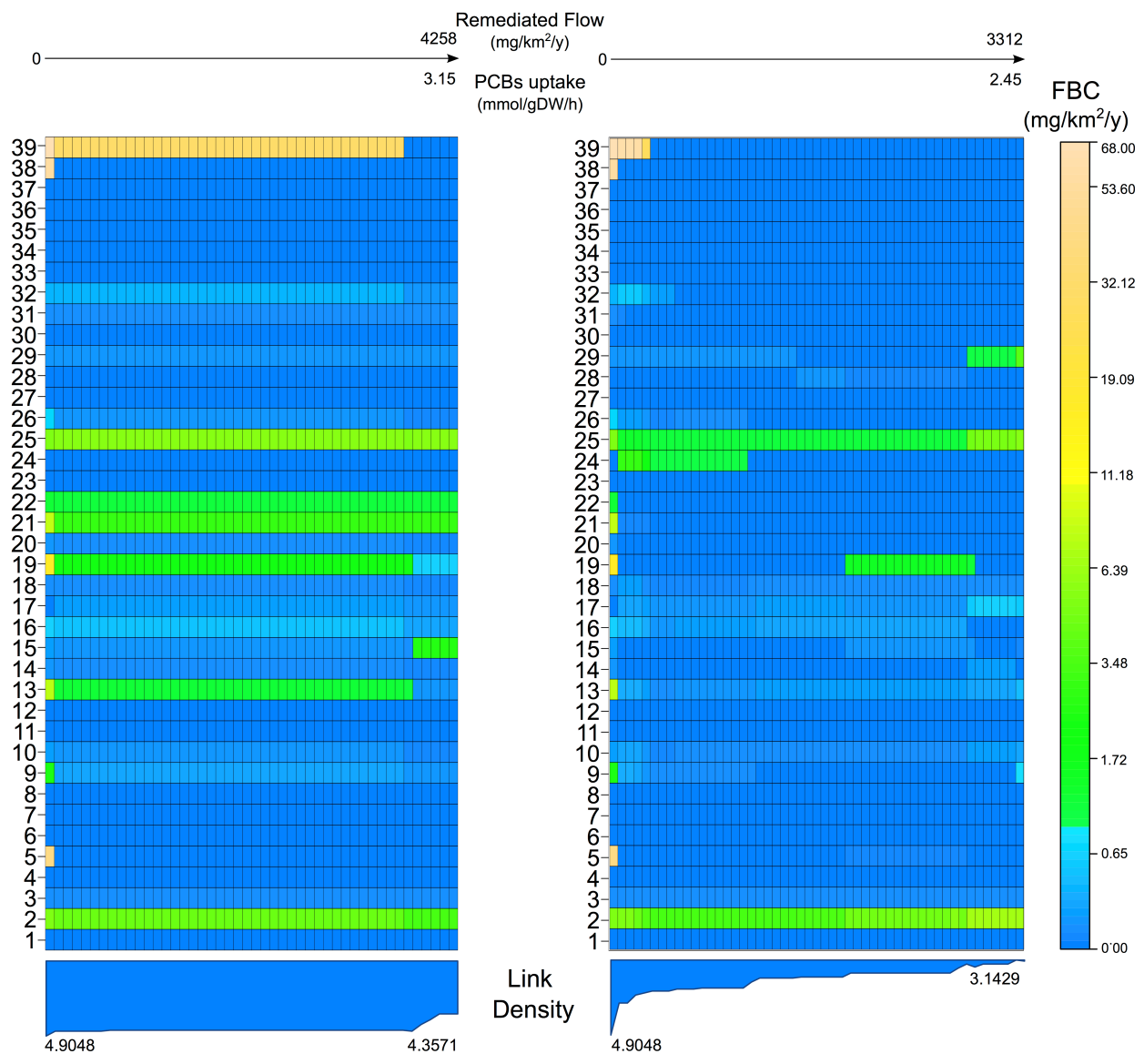
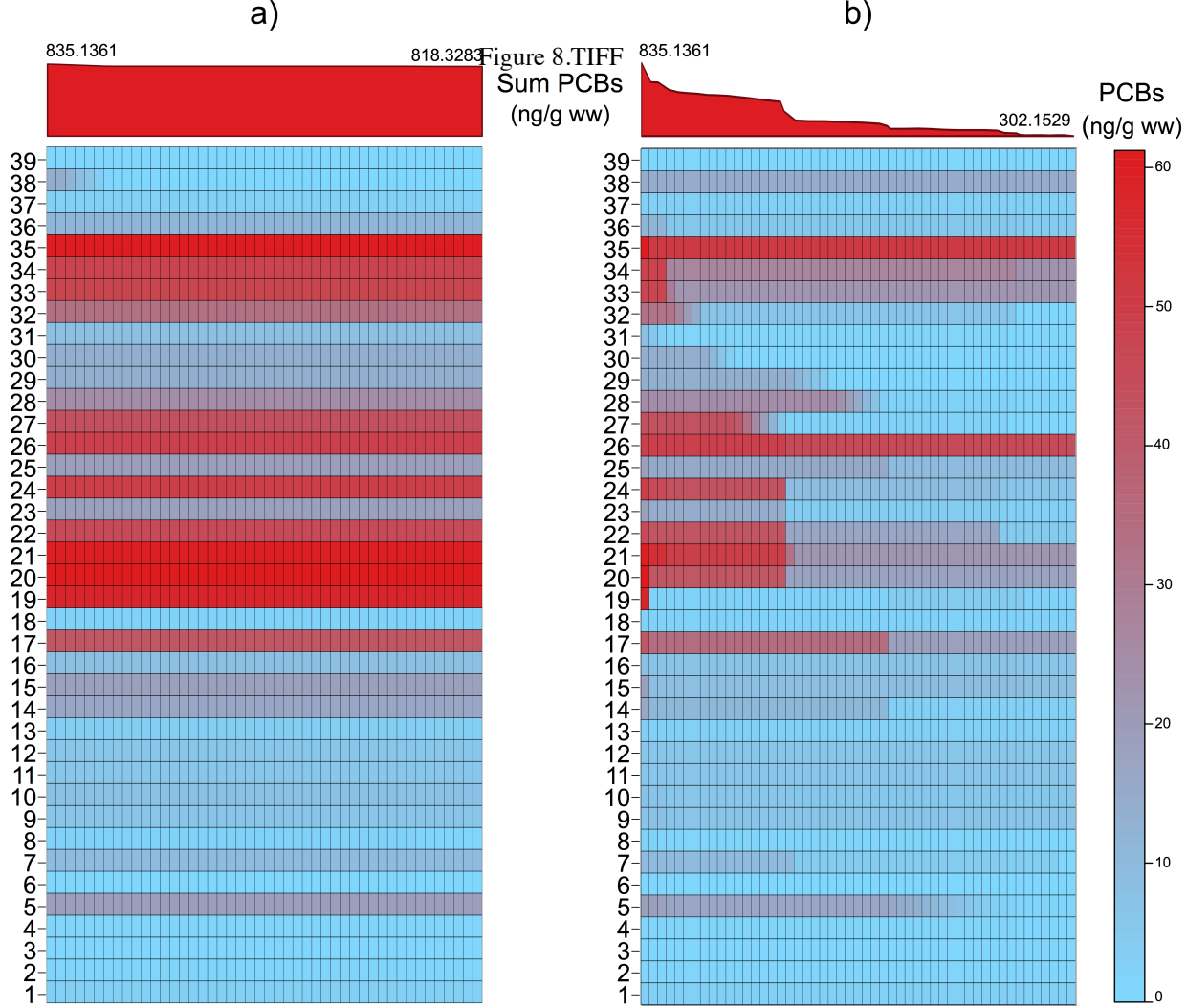


Figure 7.TIFF





- 1 Phytoplankton
2 Micro and mesozooplankton
3 Macrozooplankton
4 Jellyfish
5 Suprabenthos
6 Polychaetes
7 Commercial bivalves
8 Benthic Invertebrates
9 Shrimps
10 Norway lobster
11 Mantis shrimp
12 Crabs
13 Benthic cephalopods
14 Squids
15 Hake 1
16 Hake 2
17 Other gadiformes
18 Red mullets
19 Conger eel
20 Anglerfish
21 Flatfish
22 Turbot and brill
23 Demersal sharks
24 Demersal skates
25 Demersal fish 1
26 Demersal fish 2
27 Bentopelagic fish
28 European Anchovy
29 European Pilchard
30 Other small Pelagic Fish
31 Horse Mackerel
32 Mackerel
33 Atlantic bonito
34 Large Pelagic Fish
35 Dolphins
36 Loggerhead turtle
37 Sea birds
38 Discard
39 Detritus